Propagation of waves in high Brillouin zones: Chaotic branched flow and stable superwires

Alvar Daza[a,b,1] , Eric J. Heller[a,c], Anton M. Graf[d] , and Esa Räsänen[a,e]

[a]Department of Physics, Harvard University, Cambridge, MA 02138; [b]Nonlinear Dynamics, Chaos and Complex Systems Group, Departamento de Física, Universidad Rey Juan Carlos, Madrid 28 933, Spain; [c]Department of Chemistry and Chemical Biology, Harvard University, Cambridge, MA 02138; [d]Harvard John A. Paulson School of Engineering and Applied Sciences, Harvard University, Cambridge, MA 02138; and [e]Computational Physics Laboratory, Tampere University, Tampere 33720, Finland

We report unexpected classical and quantum dynamics of a wave propagating in a periodic potential in high Brillouin zones. Branched flow appears at wavelengths shorter than the typical length scale of the ordered periodic structure and for energies above the potential barrier. The strongest branches remain stable indefinitely and may create linear dynamical channels, wherein waves are not confined directly by potential walls as electrons in ordinary wires but rather, indirectly and more subtly by dynamical stability. We term these superwires since they are associated with a superlattice.

branched flow | superlattices | chaos | wave dynamics

Branched flow is a common phenomenon of wave dynamics; when a wave impinges a weakly refractive medium, it can create an intensity pattern akin to the shadow of a tree (1). Unlike normal diffusion, some of the (temporarily and accidentally) stable branches can carry a high density of flux across long distances. Branched flow is important on hugely disparate scales, from electron waves in two-dimensional (2D) electron gas (2) to acoustic waves spanning thousands of kilometers in the oceans (3) or the beautiful patterns of light going through soap bubbles (4). All these phenomena in both classical and quantum systems arise from wave propagation in random potentials.

As a general rule, branched flow for waves appears when the wavelength λ_F is shorter than the typical length scale a of the potential given small angle deflections per "feature" in the potential. In most materials, the lattice constants are of the order of angstroms, whereas the electron wavelengths are in the nanometer scale (i.e., $\lambda_F > a$), so we may expect that branched flow cannot exist in crystals. However, in recent years, much attention has been given to superlattices, where the combined periodic structures may create a larger-scale periodic structure. A perfect example is twisted bilayer graphene that exhibits a large-scale moiré pattern (5) and exotic properties such as superconductivity (6–10). As the condition $\lambda_F < a$ in these superlattices is generally satisfied, the branched flow can provide important understanding on the physical properties of "designer materials," including layered structures (11–13), artificial lattices (14–17), and photonic systems (18). We remark that in perfect superlattices, the branched flow is "lurking" in Bloch waves, which can be made from branched flow waves and vice versa.

In this work, we extend the concept of branched flow to periodic potentials. Thus, we demonstrate the ubiquity of branched flow from classical and quantum scales and from random disorder to periodic systems. However, perhaps even more important than these irregular patterns are the indefinitely stable branches that can arise in periodic potentials. Within these controlled branches, propagating waves are dynamically confined, creating superwires. Unlike wires based on energetic barriers, these superwires arise because of the dynamics. In this regime, waves could surmount the poten-tial barrier, but their dynamics keep them in a narrow spatial region.

The paper is organized as follows. In *Methods*, we outline the computational methods employed in the study of branched flow in both classical and quantum regimes, which share many features in the semiclassical limit. In *Branched Flow in Periodic Systems*, we demonstrate the appearance and properties of branched flow in periodic systems compared with the conventional branched flow and the Bloch wave representation. Further, in *Dynamics of Branched Flow*, we examine the classical picture that provides insight about the origin of branched flow and its relation to chaos. Channeling effects in terms of long-lived stable branches are studied in detail in *Stability and Superwires*. Finally, the possible implications of our findings and the future directions are discussed in *Discussion*.

Methods

Branched flow is typically examined by classical trajectories and by time-dependent wave packet calculations under the influence of random potentials (19). For periodic superlattices, we also use both classical and wave packet analyses, finding both branched and superwire flow. The 2D results are supplemented by the simpler one-dimensional (1D) "kick and drift" map, aiding understanding of branching and superwire dynamical channeling.

The evolution of the wave packet is computed using the split-operator technique (20). This iterative method comprises several steps. 1) The initial state evolves under the action of the potential in the coordinate

---

Significance

Waves propagating through random media can accumulate in strong branches, intensifying fluctuations and powerful phenomena such as tsunamis. However, branched flow is not restricted to the large scale, and here, we find surprisingly that branched flow is not restricted to random media. We show that quantum waves living in the high Brillouin zones of periodic potentials also branch. Moreover, some of these branches do not decay as in random media but remain robust indefinitely, creating dynamically stable channels that we call superwires. The waves in these stable branches have enough energy to surmount the channel potential and go elsewhere, but classically, nonlinear dynamics keeps them confined within the channel. These results have direct experimental consequences for superlattices and optical systems.

ENGINEERING

representation $\Psi \rightarrow e^{-iV(q)\tau/\hbar}\Psi$, 2) the resulting state is Fourier transformed into momentum representation $\Psi \rightarrow \hat{\Psi}$, 3) the state evolves in the momentum representation $\hat{\Psi} \rightarrow e^{-ip^2\tau/2m\hbar}\hat{\Psi}$, and 4) an inverse Fourier transform gives back the resulting state to the coordinate representation $\hat{\Psi}(t + \tau) \rightarrow \Psi(t + \tau)$. This procedure provides a fast and reliable method to study the wave dynamics, as long as the time step τ is small. In fact, most of the pictures depicted here were computed within a few minutes in a regular workstation.

If the quantum wavelength is short enough, the semiclassical approach will be valid, making a classical analysis very informative even though the goal is to understand quantum systems. We study the density of a large ensemble (typically thousands) of classical trajectories using initial distributions analogous to the quantum ones. Given the Hamiltonian nature of the problem, integration is carried out with a symplectic scheme (21, 22) preserving the phase-space volume and the energy in all cases. We employ a computational cluster to perform the classical simulations in reasonable times.

Branched Flow in Periodic Systems

Fig. 1A shows conventional branched flow in a 2D potential characterized by randomly positioned wells (gray dots). The initial state corresponds to a narrow Gaussian wave packet localized at the center. The wells are modeled by soft Fermi-type potentials (ref. 23 and below) with an amplitude that corresponds to half of the energy of the wave packet. The characteristics of the branching produced by this random potential are similar to the previous findings (1).

In Fig. 1 B–D, the potential is similar to Fig. 1A, but the wells are arranged in a periodic triangular lattice. Intuitively, we may expect the system to be characterized by Bloch waves—Fig. 1B has an example. However, the propagation of the wave packet under the periodic potential leads to branched flow that is astonishingly similar to conventional branched flow; Fig. 1 C and D is discussed in detail below. Fig. 1, *Insets* show the momentum Fourier transform of the corresponding panels. This representation does not correspond exactly to the reciprocal space (we would need to make Bloch wave Fourier transformation), but it helps to understand the different regimes.

First, Fig. 1C shows a snapshot of the full wave packet during the evolution. The components with short wavelengths propagate faster, whereas the components with longer wavelengths lag behind and remain closer to the origin. As the wave evolves, its Fourier transform $\Psi_E = \int_{-\infty}^{\infty} e^{-iEt/\hbar} dt$ for some particular energy E can be accumulated. For sufficiently large lattices, waves exiting the observation window never return. This means that the integral over infinite time can be reduced to the observation time that each component of the wave packet takes to leave the picture. By using an absorbing potential around the observation window, the filtered state Ψ_E is an eigenfunction by construction, but its morphology can be very complicated without spatial periodicity as in the Bloch wave.

Fig. 1D shows an eigenfunction constructed by Fourier transform of the wave packet in Fig. 1C. Chaotic branching similar to conventional branched flow in Fig. 1A is clearly visible. Some branches are localized on top of the bumps, whereas others are avoiding them. This can be a hint for the presence of quantum scars (24–26). Classically, these regions correspond to unstable periodic orbits of chaotic systems. Such unstable trajectories belong to a set of measure zero in the classical picture, but
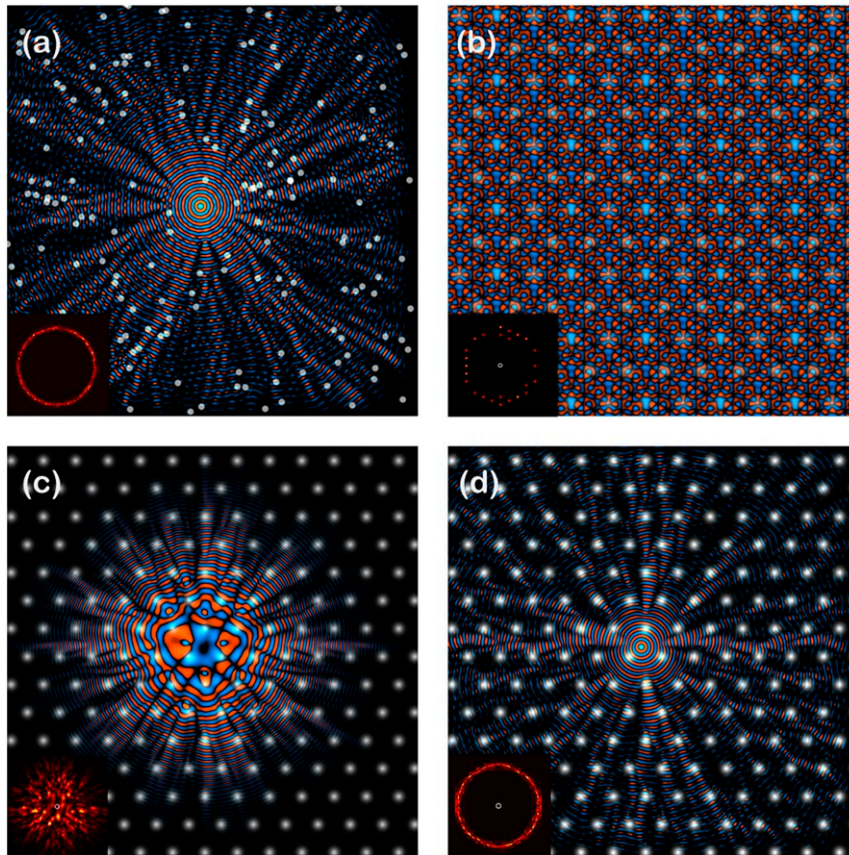

Fig. 1. The real part of different quantum waves (red for the positive and blue for the negative). White dots show the underlying potential. (*A*) Branched flow in a potential made out of randomly spaced wells. (*B*) Bloch wave ($\vec{k} = \vec{0}$) for a triangular potential. (*C*) Snapshot of a Gaussian wave packet evolving in a triangular superlattice. The fast components lead the evolution of the wave on the periphery, while the slower components lag near the center. (*D*) Eigenfunction of the wave packet of *C* made using an energy Fourier transform. *Insets* show the momentum representation of the corresponding panels.

surprisingly, the probability of the quantum wave is enhanced in these regions.

As another feature in Fig. 1, several wavelengths can fit in between consecutive bumps. This indicates that these branched eigenfunctions live far beyond the first Brillouin zone. Of course, everything can be folded into the first Brillouin zone, but we might lose some intuition by such an operation. Nevertheless, the requirement $\lambda_F < a$ discussed above is clearly fulfilled, and it has direct relevance for, for example, twisted bilayer graphene and other moiré superlattices (5–10).

Next, we focus on the role of the periodic potential in branching and on the complementarity between branched eigenfunctions and Bloch waves. Fig. 2 shows a comparison between the evolution of a wave in a periodic triangular potential (gray scale) and in free space without the potential (color scale). The black circle in the middle corresponds to an absorbing potential. In Fig. 2A, the initial state is a wave packet with downward momentum, whereas in Fig. 2B, the initial state is a Bloch wave, which is also descending. In both cases, the free wave casts a relatively hard shadow, devoid of color, as it passes beyond the absorbing hole. Instead, the periodic potential injects clear branches (gray scale) behind the disk. This is not diffraction but rather, a consequence of motion that would also be present classically. In the case of Fig. 2B, it is seen that the Bloch wave hides the underlying branched flow "fabric." This illustrates the complementarity of Bloch waves and branched eigenfunctions displayed along this work. Indeed, we can think of Bloch waves as the analog of plane waves in periodic structures; it is noticeable that many interesting and useful linear combinations of plane waves are constructed, but this approach has been much less exploited in the context of Bloch waves.

Fig. 2A shows more surprising effects. For example, the periodic potential eventually leads to backward propagation, which is prominent in the upper right corner. In the same region, we can also clearly see the periodic structure resulting from the triangular potential. Such regular patterns may emerge depending on boundary conditions, here quantum point contact injection. Finally, on the right side of the colored region, we find a relatively straight branch in light gray that has a transverse node running longitudinally in between. This region is a dynamical channeling effect analyzed in detail in *Stability and Superwires*.

Dynamics of Branched Flow

Integrable and Nonintegrable Potentials. Even though the results above show that branched flow can be found in both randomized and periodic potentials, the effect applies only for sufficiently high energies compared with the underlying potential (19). Otherwise, the flow is trapped in the troughs of the potential, and the dynamics is characterized by different types of classical diffusion (sub, normal, super, anomalous) and Lévy flight behavior depending on the system parameters (23, 27, 28). Furthermore, branched flow also requires the wavelength to be sufficiently small compared with the scale of the potential. As discussed above, branched flow can happen in superlattices where the typical electron wavelength λ_F is much smaller than the superlattice spacing a, $\lambda_F \gg a$. If the wavelength is comparable with or even larger than the lattice spacing, the wave ignores the potential just as light becomes transparent through window glass. However, other than these requirements, there is another important ingredient that has not been explicitly studied before (i.e., the integrability of the potential).

In Fig. 3, we compare the dynamics of the wave packet in both classical (Fig. 3 A and B) and quantum (Fig. 3 C and D) simulations using both integrable (Fig. 3 A and C) and nonintegrable (Fig. 3 B and D) potentials. The integrable potential is defined as $V = -A(\cos x + \cos y)$, which corresponds to a square lattice that is revealed by the darker regions of the picture. For this potential, the motion can be separated into x and y in terms of Jacobi elliptic functions. The density of classical trajectories in Fig. 3A shows focusing of the beam along the four main channels, the pattern is repetitive and predictable. After a trajectory enters one of these channels, it remains confined within its narrow boundaries as long as the potential remains periodic. This kind of behavior has been previously studied for waves propagating through media with sinusoidal variations of the refractive index (29).

In comparison, Fig. 3B shows the density of classical trajectories in a nonintegrable Fermi-type potential defined as $V(\vec{r}) = \sum_{j=1}^{N} A/[1 + \exp(|\vec{r} - \vec{r}_{0j}|/\sigma)]$, which is also used above within Figs. 1 and 2. Now, $\vec{r}_{0j}$ provides the location of each of the N bumps of a square lattice (gray dots). In this case, a more intricate pattern emerges, including branches showing up at nontrivial locations and carrying a high density of flow along variable lengths. The drastic difference from an integrable case in Fig. 3A shows that the nonintegrability—corresponding to a chaotic system—is the key ingredient behind branched flow. This is demonstrated also by the phase-space pictures given as Fig. 3 A, *Inset* and B, *Inset*; foci arise as a consequence of cusp catastrophes, which can occur in integrable and chaotic dynamics, but the distribution and stability of these foci are much richer when the phase space is scrambled, corresponding to a branched flow.

In Fig. 3 C and D, we show that the corresponding densities of quantum wave functions evolved under the same integrable and
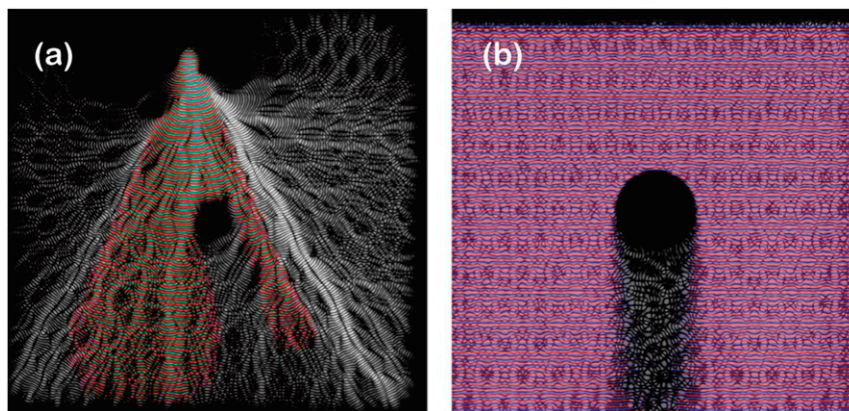

Fig. 2. Illustration of the Bloch wave–branched eigenfunction duality. (A) Wave packet propagation with downward initial momentum in a triangular potential (gray scale) exposed to an absorbing disk at the center of the figure. The colors correspond to the same propagation but in free space without the triangular lattice. *B* is the same as in *A*, but now, the initial state is a Bloch wave. The absorbing disk casts a shadow for the free wave (no color after the disk), but this space is filled by branches when the triangular potential is present (gray tendrils).
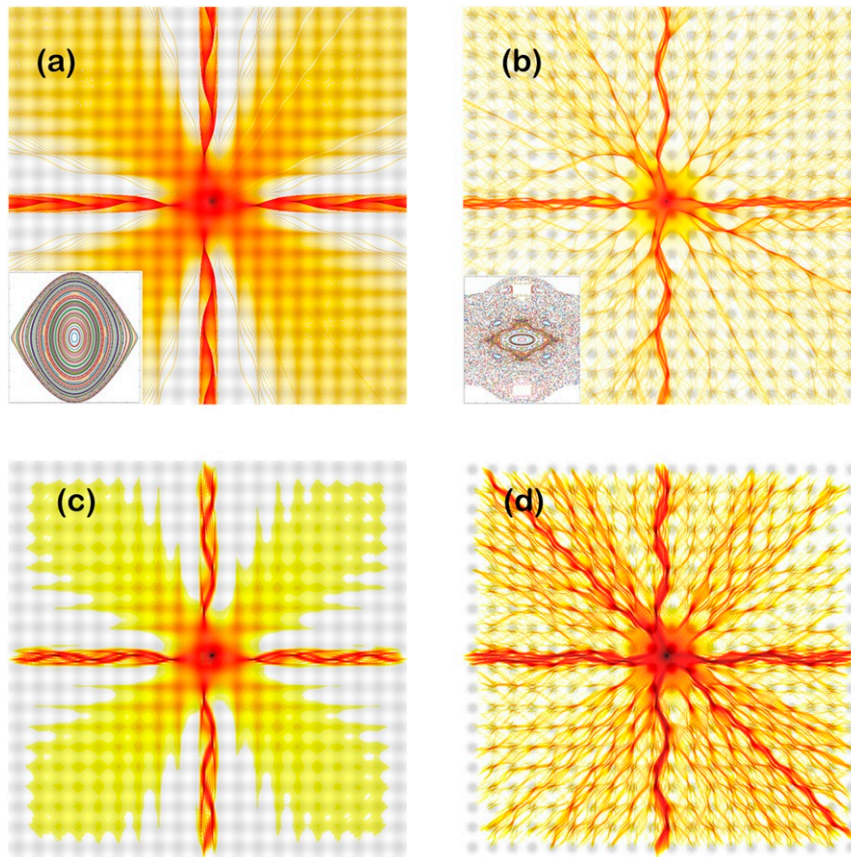
Fig. 3. The role of chaos in branched flow. (*A*) Density of classical trajectories in a square lattice defined by an integrable potential. (*B*) The same as in *A* but in a nonintegrable potential. The *Insets* of *A* and *B* show the respective Poincaré sections, displaying periodic orbits in the integrable potential and a mixed phase space (chaotic sea with periodic islands) for the nonintegrable case. (*C*) Density of a quantum wave function in an integrable potential. (*D*) The same as in *C* but in a nonintegrable potential.

nonintegrable potentials, respectively. The agreement between the classical and quantum simulations is evident, as well as the differences between the integrable and nonintegrable potentials. Among other details, we can observe that the Pearcey diffraction pattern (30) arises in the integrable case of Fig. 3*C* (although it is hard to see because of the asymmetrical launching), while the pattern is completely obscured in the nonintegrable case in Fig. 3*D*. Despite being common for individual cusps (31), Pearcey patterns are not expected to be visible in branched flow in general, where many features (including other cusps) coexist in the vicinity of the cusps.

Hence, these results demonstrate that the main ingredients required for the phenomenon of branched flow are similar both classically and quantum mechanically. In particular, the nonintegrability of the potential is a necessary condition—and also, the default condition from an experimental perspective. Furthermore, the characteristics of the main and secondary branches in classical and quantum cases are very much alike, as clearly seen in Fig. 3.

Kick and Drift Map. To analyze the branched flow in a periodic system further, let us consider the classical kick and drift map (1). It is an area-preserving time-discrete map based on Hamilton's equation of motion defined by

$$p_{n+1} = p_n - \frac{\partial V}{\partial x}\bigg|_{x=x_n},$$
$$x_{n+1} = x_n + p_{n+1},$$
[1]

where x and p correspond to the trajectory's position and transverse momentum, respectively; n is a natural number playing the role of discrete time; and V is a potential depending on the position. The kick and drift map receives its name because of its two stages; first, the momentum changes according to the potential, and then, the trajectory drifts until the next kick. This simple picture provides useful insights about the phase-space transformations that give rise to branched flow, including the creation of foci through cusps and the stability of the long-lived branches, among other interesting effects.

Previously (1), the "kick" used randomly chosen parameters, but here, we repeatedly use the same spatially periodic potential, writing

$$p_{n+1} = p_n + K\sin x_n,$$
$$x_{n+1} = x_n + p_{n+1},$$
[2]

where K accounts for the height of the potential. Eq. **2** defines the celebrated standard map, studied by Boris Chirikov in the context of Hamiltonian chaos and the Kolmogorov–Arnold–Moser theory (32, 33). For low values of the perturbation strength K, periodic motion dominates, whereas for higher values, the phase space increasingly fills with chaotic trajectories. This kind of map can be connected to quantum mechanics through Wigner transformation (34), where phase space is coarse grained by Planck's constant smoothing out of fine details but keeping much of its rich structure. Stable islands in the standard map concentrate the density of trajectories in particular regions of phase space. Indeed, it has been proven that strong branches typically match areas with low rarefaction exponent (35). In
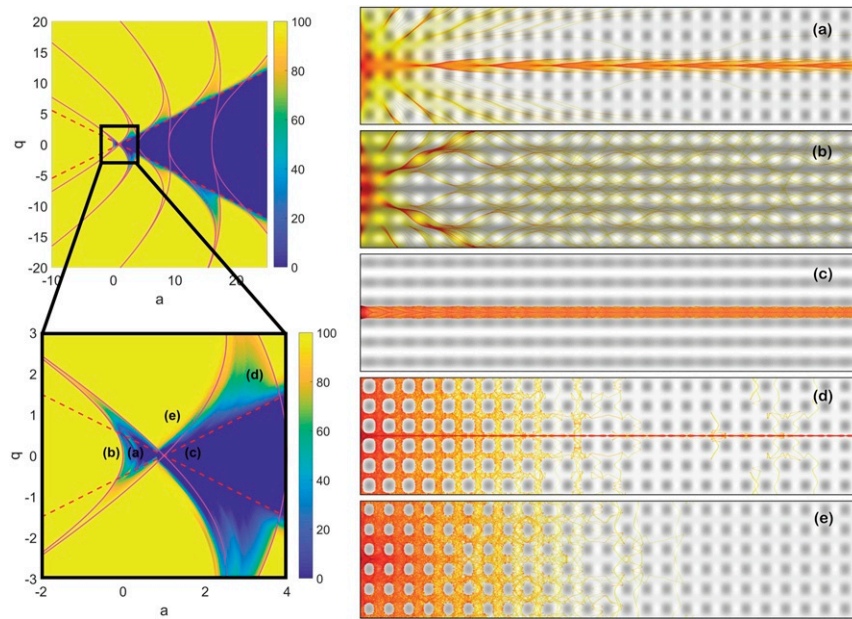
Fig. 4. (*Left*) The stability diagram for the potential of Eq. **4**. The color code shows the percentage of trajectories that remain within the initial channel from an initial wedge spanning 60°. The magenta lines are for the stability of Eq. **3**, while the red dashed lines are for $q = (1 - a)/2$ and $q = (a - 1)/2$ to help identify the different regions in terms of energy. (*A*) Classical simulation of a superwire, where trajectories remain confined due to the dynamics. For parameters in *B*, the horizontal channel is not populated. (*C*) Energetically confining channel. Trajectories cannot surmount the barriers. (*D*) Trajectories can escape in between the bumps but cannot override them. The dynamical confinement is not as strong as the one in *A*. (*E*) Trajectories explore the potential chaotically.

random potentials, these stable regions exist just for a finite period of time, but in periodic potentials, they remain indefinitely stable, corresponding to channels or superwires. This mechanism complements the caustic formation as main justifications of branch formation. Therefore, we can classify branches as R branches, if low rarefaction creates the accumulation of flow, or C branches, if it is caustics that generate the higher intensity. Nevertheless, both mechanisms are typically at play at the same time, and it is hard to uniquely label them.

Stability and Superwires

According to our results above, branched flow appears when a classical or quantum wave with sufficient energy impinges on potential landscape (periodic or not)—as long as the potential is not integrable. By examining Fig. 3, we can see that the four arms of the cross both in the integrable and in the nonintegrable cases remain stable for long times. Here, we will refer to these regions where the flow remains bounded for long times as channels or superwires, because of their relation to superlattices. Recent developments in optical lattices have also arrived at several ways to produce nondiffractive beams in periodic systems (36), even under more general conditions such as accelerating beams (37–39). Thus, there is an interesting analogy between different fields of physics. Here, however, we study particles with mass using the time-dependent Schrödinger equation and consider a smooth perturbative potential. This is conceptually different from considering light beams in photonic crystals using Maxwell's equations.

The stability of the channels can be understood in terms of motion normal to the superwire paths, which can be approximated by Mathieu functions (40, 41). Consider a classical trajectory starting in the center of a square lattice of repulsive soft pillars, heading to the right between the rows of bumps (Fig. 4 shows an example). As the trajectory progresses, its motion can be linearized around the exact, straight line path down the bumpy rows. By symmetry, the path has no transverse force on it, and it

remains straight. A stability analysis is needed to determine the fate of nearby trajectories. If they are stable, there are superwire paths oscillating down the row. Expanding the potential to second-order normal to the path, the effective potential is a harmonic oscillator with a force constant that is varying (nearly) periodically. If that variation is approximately sinusoidal, the stability can be assessed with the Mathieu equation:

$$\frac{d^2x}{dt^2} + (a - 2q\cos 2t)x = 0. \tag{3}$$

The stability of the solutions of this equation has been thoroughly studied (41). If the time variation has strong harmonics, the analysis and the results are similar, so we are content with the Mathieu analysis for now.

The key to the stability is the period π of the oscillation of $2q\cos 2t$ relative to the time-averaged frequency $\sqrt{a}$. A channel trajectory is equivalently parameterized by a fixed a, given by the shape of the potential normal to the path. Thus, we can write Eq. **3** as $d^2x/dt^2 + (a - 2q\cos 2\omega t)x = 0$, where $\omega = 2\pi/\tau$ and $\tau = A/v$ is the time to traverse a unit cell of width A at velocity v. The velocity of the flow down the superwire relative to the superlattice parameters becomes crucial. At high velocity, the method of averaging suggests that the trajectory will always become stable. The Mathieu stability diagram confirms this with ever-narrowing resonances and larger regions of stability with increasing speed (increasing ω).

Even if the velocity v is not adjustable, as is the case for electrons in twisted bilayer graphene away from the flat band region, the frequency ratio can be controlled by the twist angle, thus adjusting A in $\sqrt{a}/\omega = \sqrt{a}/(2\pi v/A)$. Or, in artificial superlattices, it can be controlled by fabrication geometry. The stability and time dependence of a quantum version of the Mathieu problem are exactly the same as the classical because it is a harmonic oscillator, a linear dynamical system. Thus, the classical stability analysis is directly related to the quantum evolution,

Daza et al.
Propagation of waves in high Brillouin zones: Chaotic branched flow and stable superwires

PNAS | 5 of 7
https://doi.org/10.1073/pnas.2110285118

as confirmed for example in Fig. 3. We can test these ideas by constructing a 2D potential with analogous properties to the 1D standard map. The potential is given by

$$V = -(2q \cos 2x - a) \sin y^2. \qquad [4]$$

Here, we have sinusoidal wells instead of harmonic, but by Taylor expansion, they are well approximated as harmonic at $y = n\pi$, $n \in \mathbb{Z}$. By computing the evolution of a classical manifold, we can see how many trajectories remain within the boundaries of their initial channels after a long time. This is represented in Fig. 4. The magenta lines show the stability lines for Eq. **3** in agreement with the simulations. The red dashed lines help us to understand the relation between the kinetic and potential energy. Fig. 4 *A* and *B* is on the only part of the (a, q) stability region where trajectories can override the bumps. However, the dynamics of trajectories in Fig. 4*A* keeps them within the channel, thus creating a classical superwire. The periodicity of the focusing of the trajectories is incommensurate with respect to the periodicity of the potential. This is precisely what makes the channel stable; otherwise, the trajectories would be resonant and leave it.

The superwires should not be confused with channels that are trapped energetically (i.e., confined by the bumpy potential). This regime occurs for parameters (a, q) in the region between $q > (T - a)/2$ and $q < (a - T)/2$, where T is the initial kinetic energy (in Fig. 4, we have chosen the kinetic energy $T = 1$, and this energetically trapping region corresponds to the big blue triangle on the right side of the stability plot). As shown in Fig. 4*C*, trajectories in such regime cannot surmount the potential barrier, and consequently, they are restricted to a nearly 1D space. Considering a many-body problem, this situation could lead to a Luttinger liquid with correlated electrons, but our present study is restricted to the one-body problem of a particle in a superlattice.

Fig. 4 *D* and *E* shows an intermediate regime, where trajectories can escape in between the bumps but cannot ride over the top of them. Some trajectories in these dynamical channels leak out, unlike superwires as the one shown in Fig. 4*A*. For such values of the energy, other diffusive mechanisms are at play (23, 27, 28), hampering controlled transport of the flow.

Different potentials could be built where superwires would be the dominant regime in the parameter space. The potential of Eq. **4** is specifically designed to mimic the stability of the Mathieu equation, but for example, variations on the Fermi potential discussed above would also be ruled by the Mathieu equation in the vicinity of the minimum (maximum) between the bumps (wells).

Finally, we demonstrate the formation of superwires in a quantum mechanical calculation. Fig. 5 shows an example of a wave

packet propagation from the left into a square lattice. The wave packet is Fourier transformed from time to energy at a chosen energy, which reveals a dynamically stable superwire along the channel between the bumps. However, if the lattice was extended farther to the right, tunneling to the neighboring parallel channels would eventually occur. This dynamical tunneling (42) would correspond to the existence of a flat electronic band along the $\vec{k}$ direction normal to the channel. It is easy to imagine ways to prevent this dynamical tunneling from happening, like creating uneven channels. Different injections could also be used to control the population of the branches (43).

Discussion

The results of this work connect and complete different areas in nonlinear dynamics. Varying the energy of classical trajectories and quantum mechanical wave packets in periodic potentials gives rise to multiple dynamical regimes. Different kinds of classical diffusion have been reported for values of the energy comparable with or below the potential barriers (23, 27, 28). At higher energies, typically several times larger than the height of the potential, we find the branched flow regime as demonstrated here for a periodic potential. In branched flow, individual trajectories fly over the potential and are barely affected by it, but successive interactions force the manifolds to fold onto themselves, creating cusps and stable regions in phase space that give rise to the branches. Moreover, by using periodic potentials, the connection between classical chaos and branched flow has become evident. However, there is a crucial difference of perspective compared with most of the standard map chaos literature; we focus on the early and medium time development, or temporal evolution, of the phase-space structure, as in the study of branched flow.

The ideas presented here also lead to important questions in condensed matter physics. Branched flow is a transient regime in time and space, so electrons will eventually resemble Bloch waves. However, it may well be the case that this transient behavior dominates for very long distances and lives for very long times. In particular, superwires demonstrated here can remain stable almost forever, except possibly for tunneling. Electrons traveling through these dynamical channels of the superlattices would have zero resistivity. Although the persistence of the channels under perturbations still needs to be studied, it is hard to imagine how phonons could interact with electrons in these superwires.

The connections of the present ideas to other areas of physics, such as photonics or experiments with cold atoms, open questions too. For example, manufactured waveguides allow bending light in photonic crystals (44). It would be interesting to investigate if superwires can curve too by slow variation of the lattice parameters. A quantum wave in a channel is not confined there forever; tunneling will occur, providing flux to adjacent channels. This is required of a periodic potential, but the band energy is nearly flat in the direction perpendicular to the propagation. Tunneling will be slow, and since the classical motion is stable, with no potential barrier, this is "dynamical tunneling." The role of dynamical tunneling and chaos-assisted tunneling (45) in the superwire regime should also be studied in future works.
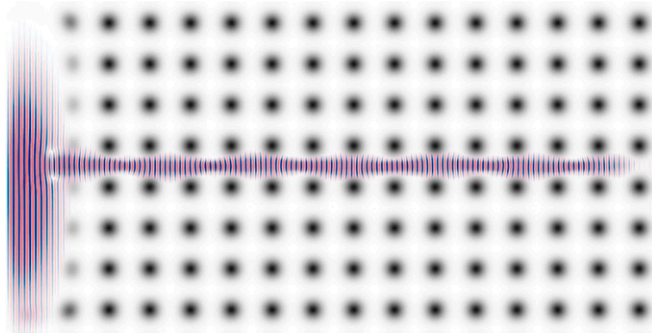
Fig. 5. Example of a stable superwire. A quantum wave packet is injected from the left into the square lattice. A Fourier transform at a chosen energy reveals dynamical stability along the channel for the chosen parameters. Notice the difference between the periodicity of the propagating wave and the periodicity of the potential.

1. E. J. Heller, R. Fleischmann, T. Kramer, Branched flow. arXiv [Preprint] (2019). https://arxiv.org/abs/1910.07086 (Accessed 10 September 2021).
2. M. A. Topinka et al., Coherent branched flow in a two-dimensional electron gas. Nature 410, 183–186 (2001).
3. H. Degueldre, J. J. Metzger, T. Geisel, R. Fleischmann, Random focusing of tsunami waves. Nat. Phys. 12, 259–262 (2016).
4. A. Patsyk, U. Sivan, M. Segev, M. A. Bandres, Observation of branched flow of light. Nature 583, 60–65 (2020).
5. R. Bistritzer, A. H. MacDonald, Moire bands in twisted double-layer graphene. Proc. Natl. Acad. Sci. U.S.A. 108, 12233–12237 (2011).
6. Y. Cao et al., Unconventional superconductivity in magic-angle graphene superlattices. Nature 556, 43–50 (2018).
7. Y. Cao et al., Correlated insulator behaviour at half-filling in magic-angle graphene superlattices. Nature 556, 80–84 (2018).
8. M. Yankowitz et al., Tuning superconductivity in twisted bilayer graphene. Science 363, 1059–1064 (2019).
9. X. Lu et al., Superconductors, orbital magnets and correlated states in magic-angle bilayer graphene. Nature 574, 653–657 (2019).
10. P. Stepanov et al., Untying the insulating and superconducting orders in magic-angle graphene. Nature 583, 375–378 (2020).
11. K. Kim et al., Tunable moiré bands and strong correlations in small-twist-angle bilayer graphene. Proc. Natl. Acad. Sci. U.S.A. 114, 3364–3369 (2017).
12. P.-Y. Chen et al., Tunable moiré superlattice of artificially twisted monolayers. Adv. Mater. 31, e1901077 (2019).
13. A. Tartakovskii, Excitons in 2D heterostructures. Nat. Rev. Phys. 2, 8–9 (2019).
14. K. K. Gomes, W. Mar, W. Ko, F. Guinea, H. C. Manoharan, Designer Dirac fermions and topological phases in molecular graphene. Nature 483, 306–310 (2012).
15. M. Polini, F. Guinea, M. Lewenstein, H. C. Manoharan, V. Pellegrini, Artificial honeycomb lattices for electrons, atoms and photons. Nat. Nanotechnol. 8, 625–633 (2013).
16. M. R. Slot et al., Experimental realization and characterization of an electronic Lieb lattice. Nat. Phys. 13, 672–676 (2017).
17. A. A. Khajetoorians, D. Wegner, A. F. Otte, I. Swart, Creating designer quantum states of matter atom-by-atom. Nat. Rev. Phys. 1, 703–715 (2019).
18. A. Reserbat-Plantey et al., Quantum nanophotonics in two-dimensional materials. ACS Photonics 8, 85–101 (2021).
19. E. J. Heller, The Semiclassical Way to Dynamics and Spectroscopy (Princeton University Press, 2018).
20. M. D. Feit, J. A. Fleck Jr., A. Steiger, Solution of the Schrödinger equation by a spectral method. J. Comput. Phys. 47, 412–433 (1982).
21. L. Verlet, Computer "experiments" on classical fluids. I. Thermodynamical properties of Lennard-Jones molecules. Phys. Rev. 159, 98 (1967).
22. H. Yoshida, "Recent progress in the theory and application of symplectic integrators" in Qualitative and Quantitative Behaviour of Planetary Systems, R. Dvorak, J. Henrard, Eds. (Springer, 1993), pp. 27–43.
23. R. Klages, S. S. G. Gallegos, J. Solanpää, M. Sarvilahti, E. Räsänen, Normal and anomalous diffusion in soft Lorentz gases. Phys. Rev. Lett. 122, 064102 (2019).
24. L. Kaplan, Scars in quantum chaotic wavefunctions. Nonlinearity 12, R1 (1999).
25. P. J. Luukko et al., Strong quantum scarring by local impurities. Sci. Rep. 6, 37656 (2016).
26. J. Keski-Rahkonen, A. Ruhanen, E. J. Heller, E. Räsänen, Quantum Lissajous scars. Phys. Rev. Lett. 123, 214101 (2019).
27. G. Cristadoro, T. Gilbert, M. Lenci, D. P. Sanders, Machta-Zwanzig regime of anomalous diffusion in infinite-horizon billiards. Phys. Rev. E Stat. Nonlin. Soft Matter Phys. 90, 050102 (2014).
28. L. Zarfaty, A. Peletskyi, I. Fouxon, S. Denisov, E. Barkai, Dispersion of particles in an infinite-horizon Lorentz gas. Phys. Rev. E 98, 010101 (2018).
29. M. V. Berry, D. H. J. O'Dell, Ergodicity in wave-wave diffraction. J. Phys. Math. Gen. 32, 3571 (1999).
30. T. Pearcey, The structure of an electromagnetic field in the neighbourhood of a cusp of a caustic. Lond. Edinb. Dublin Philos. Mag. J. Sci. 37, 311–317 (1946).
31. M. V. Berry, Elementary branching: Waves, rays, decoherence. J. Opt. 22, 115608 (2020).
32. B. V. Chirikov, "Research concerning the theory of non-linear resonance and stochasticity" (Rep. CERN-Trans-71-40, CERN, Geneva, Switzerland, 1971).
33. B. V. Chirikov, A universal instability of many-dimensional oscillator systems. Phys. Rep. 52, 263–379 (1979).
34. H. J. Korsch, M. V. Berry, Evolution of Wigner's phase-space density under a nonintegrable quantum map. Physica D 3, 627–636 (1981).
35. E. J. Heller, S. Shaw, Branching and fringing in microstructure electron flow. Int. J. Modern Phys. B. 17, 3977–3987 (2003).
36. O. Manela, M. Segev, D. N. Christodoulides, Nondiffracting beams in periodic media. Opt. Lett. 30, 2611–2613 (2005).
37. R. El-Ganainy et al., Discrete beam acceleration in uniform waveguide arrays. Phys. Rev. A 84, 023842 (2011).
38. I. Kaminer, J. Nemirovsky, K. G. Makris, M. Segev, Self-accelerating beams in photonic crystals. Opt. Express 21, 8886–8896 (2013).
39. K. G. Makris et al., Accelerating diffraction-free beams in photonic lattices. Opt. Lett. 39, 2129–2132 (2014).
40. É. Mathieu, Mémoire sur le mouvement vibratoire d'une membrane de forme elliptique. J. Math. Pures Appl. 13, 137–203 (1868).
41. N. W. McLachlan, Theory and Application of Mathieu Functions (Oxford University Press, 1951).
42. M. J. Davis, E. J. Heller, Quantum dynamical tunneling in bound states. J. Chem. Phys. 75, 246–254 (1981).
43. A. Brandstötter, A. Girschik, P. Ambichl, S. Rotter, Shaping the branched flow of light through disordered media. Proc. Natl. Acad. Sci. U.S.A. 116, 13260–13265 (2019).
44. J. D. Joannopoulos, P. R. Villeneuve, S. Fan, Photonic crystals. Solid State Commun. 102, 165–173 (1997).
45. M. Arnal et al., Chaos-assisted tunneling resonances in a synthetic Floquet superlattice. Sci. Adv. 6, eabc4886 (2020).

ENGINEERING